Author Name

Data Mining in Systems Health Management

Contents

4

Chapter 1

Combined Model-based/Data-driven Approach to Failure Prognosis

Marcos Orchard

Electrical Engineering Department, Universidad de Chile, Santiago, Chile (phone: +56-2-978.42.15; e-mail: morchard@ing.uchile.cl)

George Vachtsevanos

School of Electrical and Computer Engineering, Georgia Institute of Technology, Atlanta, GA 30332, USA (e-mail: gjv@ece.gatech.edu)

Kai Goebel

NASA Ames Research Center, Moffett Field, CA (phone: +1-650-604-4204; e-mail: kai.goebel@nasa.gov)

1.1 Introduction

Failure prognosis - as a natural extension to the fault detection and isolation (FDI) problem - has become a key issue in a world where the economic impact of system reliability and cost-effective operation of critical assets is steadily increasing. Failure prognostic algorithms aim to characterize the evolution of incipient fault conditions in complex dynamic processes, thus allowing to estimate of the remaining useful life (RUL) of subsystems and compo-

nents. Several examples can be used here to illustrate the range of possible applications for these algorithms: electro-mechanical systems, continuous-time manufacturing processes, structural damage analysis, and even fault tolerant software architectures. Most of them have in common the fact that they are highly complex, nonlinear, and affected by large-grain uncertainty.

In the case of critical helicopter parts/components, failure prognosis has been addressed over the past years via a variety of model-based and data-driven approaches [3, 5, 6, 7, 10, 17, 20]. In fact, most of research has focused primarily on the analysis of vibration data and the derivation of condition indicators (CI) [17], although no major effort has been reported thus far on a systematic methodology that integrates elements of sensing, data analysis, CI selection and extraction, fault diagnosis and failure prognosis into a single platform that may be ported to existing hardware/software health monitoring systems on-board an aircraft.

The implementation of failure prognostic algorithms can be particularly challenging when real time computation is required, as in the case of tools that must be effectively and efficiently implemented on-board the aircraft, since accuracy of RUL estimates depends on the quality of long-term predictions for the dynamic system under study. Most of the current approaches in the reliability arena involve intensive computations to process large amounts of historical data, offering little room for real time adjustments on RUL estimates when the system behaves differently from what it is expected. Moreover, given that most systems depend on external inputs, the overall effect that probable future load variations would have on the faulty subsystem also needs to be considered with care. To accurately predict the RUL of a system under fault conditions, prognostic algorithms must take into account the various stresses affecting the system either environmental (wind, temperature, humidity) or associated to control efforts (load, torque, speed). Knowledge of how these varying stress levels affect the RUL of the system provide the operator with a complete picture of how the fault is progressing, which will lead to smarter decisions in control to mitigate the fault growth while also meeting the performance requirements of the system.

Learning paradigms, and other data-driven techniques, offer an invaluable opportunity for the improvement of prognostic algorithms based on either first-principles or statistical knowledge of the system. The incorporation of real time information from input/output/feature measurements, with the purpose of uncertainty representation and management, directly benefits the implementation of automated contingency management systems (ACMs), as well as other automated corrective schemes. In this sense, this chapter explores the this concept and introduces a combined model-based/data-driven approach to failure prognosis that relies on degradation models of the failing component (namely, fault models) and sequential Monte Carlo (SMC) methods for state estimation (particle filtering). This approach allows taking advantage of real-time measurements, update model and stress parameters to project the system evolution into the future.
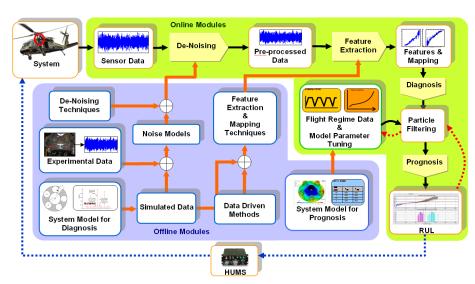
In this scheme, a particle filtering algorithm uses sequential importance sampling and Bayesian theory, combining model-based a priori information with acquired observations to approximate the state probability density function (PDF) through a set of possible realizations (particles) associated to discrete probability masses (or weights). The data-driven component of the architecture aims to account for stochastic and time-varying load profiles principal stress factors through appropriate uncertainty measures and linear interpolation techniques. These measures quantify the effect of input uncertainty on the prognostic results and are also the basis for feedback correction loops to extend the RUL of faulty nonlinear systems. Combined, the methodology addresses issues of uncertainty, system nonlinearity and non-Gaussian noise. Performance and effectiveness metrics are used to assist in the optimum design and eventual implementation of the diagnostic/prognostic algorithms and to measure the effect of input uncertainty. This unified methodology aims to improve significantly the predictive horizon in terms of accuracy and precision compared to baseline approaches. It also provides a path towards a rigorous approach to prognostics-enhanced reconfigurable or fault-tolerant control while extending the RUL of the platform to assure mission completion without compromising the safety of the vehicle. The proposed approach is tested on a critical aircraft component in order to demonstrate its efficacy.

1.2   An integrated fault diagnosis and failure prognosis architecture

We introduce in this chapter an integrated failure prognosis architecture that is applicable to a variety of aircraft systems and industrial processes [19, 21]. We are targeting a specific rotorcraft system as a prototypical testbed for proof-of-concept. Figure 1.1 depicts the overall architecture and distinguishes between the on-board and off-board modules for eventual on-platform implementation purposes.

The online modules perform raw data pre-processing, feature or CI extraction, fault diagnosis and failure prognosis that exploit available ground truth fault data, noise models, experimental data, system models and other tools offline to tune and adapt online parameters and estimate suitable mappings. The architecture suggests a hybrid and systematic approach to sensing, data processing, fault feature extraction, fault diagnosis and failure prognosis that may lead to a system hardware/software configuration implementable online in real time. The enabling technologies include such innovative features as:

(a)   Physics-based modeling of critical components/systems that will facilitate a better understanding of the physics of failure mechanisms, provide simulated data and stress factors for diagnosis and prognosis.

FIGURE 1.1: Overall architecture for implementation of fault diagnosis and failure prognosis algorithms.

(b) Novel pre-processing routines including de-noising of raw data via blind deconvolution to improve signal to noise ratio. A thorough approach to feature or condition indicator selection and extraction that forms the foundation for accurate and reliable fault diagnosis and failure prognosis.

(c) Incipient failure diagnosis and prognosis founded on concepts from physics-based models, measurements and Bayesian estimation techniques. This innovative approach takes advantage of hybrid modeling/measurements and estimation methods to manage uncertainty and provide early fault detection, isolation and prediction of the time to failure of a failing component.

We detail in the sequel the major modules of the architecture.

1.2.1 Sensing and data processing

Modern aircraft/rotorcraft and critical industrial processes are equipped with monitoring, data acquisition and data analysis hardware and software that are intended to assess the health of components/systems and inform the operator of impending failure conditions. Massive volumes of raw data can invariably accumulate from a variety of distributed sensor suites that, if left unattended, may overwhelm the available data warehousing facilities making it almost impossible to "make sense" out of these data sources. It is imperative, therefore, that data must be processed on-line or off-line to extract useful information and knowledge. Knowledge discovery, frequently called *data mining* ,

provides a promising technology to unearth valuable information from massive amounts of data. This situation is critical when (high-bandwidth) baseline and fault data, as well as usage and flight regime data, are acquired on-board an aircraft and must be processed expeditiously and accurately to support fault detection and mitigation strategies when faced with flight critical or safety critical events. The classical paradigm of $data \rightarrow information \rightarrow knowledge$ is most relevant here and requires the development and implementation of novel techniques to tradeoff information content and accuracy with computational requirements needed to arrive at the sought after information and knowledge. The "value" of this information must be assessed via appropriate performance metrics if "useful" data attributes derived through data mining tools are to describe faithfully the captured fault process. Condition indicators or features represent certain conditions under which an anomaly or abnormality in a system's operating state is detected; it is natural, therefore, that CI rather than raw data are used for fault diagnosis and failure prognosis.

Then, on the one hand, fault diagnosis can be viewed as a mapping of given CI into one of the predesigned fault classes. The same CI may be used to detect an anomaly (an unknown a priori fault condition) when compared to healthy or baseline behaviors. On the other hand, failure prognosis involves estimating the RUL of a failing component/system once a relevant fault is detected and identified. In failure prognosis problems, it is essential that a CI exhibiting a progressive nature with respect to a fault evaluation be tracked and evaluated on the basis of its contribution to accurate and precise RUL estimates. The success of diagnostic and prognostic algorithms depends highly on the quality of these CI. To extract CI that represent in a compressed form the maximum possible information content, a statistically sufficient database of both healthy and faulty data is needed. Furthermore, data acquired on-board an aircraft are severely corrupted by noise stemming from a variety of internal and external noise sources. It is necessary therefore, that raw data be processed first via de-noising algorithms in order to improve the fault signal to noise ratio.

Raw sensor data (vibration, temperature) must be processed in order to reduce the data dimensionality and improve the fault signal-to-noise ratio (SNR). Typical pre-processing routines include data compression and filtering, time synchronous averaging (TSA) of vibration data, FFTs, among others. Pre-processing methods which improve the SNR (de-noising) are particularly valuable in aircraft situations where significant noise levels tend to mask the real information. We propose a de-noising methodology based on blind deconvolution that has been applied successfully to a helicopter system under the DARPA prognosis program [23]. The process of blind deconvolution attempts to restore the unknown vibration signal by estimating an inverse filter, which is related to partially known system characteristics. This is an active field of current research in image processing [9], speech signal processing [18], but rarely applied in mechanical vibration signals. Vibration and other high-

bandwidth signals are corrupted by multiple noise sources. A simplified model for such a complex signal may be defined as:

$$s(t) = a(t)b(t) + n(t), \tag{1.1}$$

where $s(t)$ is the measured vibration signal, $b(t)$ is the noise-free un-modulated vibration signal, $a(t)$ is the modulating signal and $n(t)$ is the cumulative additive noise. This model can be written in the frequency domain as:

$$S(f) = A(f) * B(f) + N(f), \tag{1.2}$$

with $*$ being the convolution operation and $S(f)$, $A(f)$, $B(f)$, $N(f)$ are the Fourier transforms of $s(t)$, $a(t)$, $b(t)$, $n(t)$, respectively. The goal is to recover $B(f)$. We propose an iterative de-noising scheme that starts with $\overline{z}(t)$, an initial estimate of the inverse of the modulating signal $a(t)$, which demodulates the observed signal $s(t)$ to give a rough noise-free estimate of the vibration signal in the time domain as:

$$\overline{b}(t) = s(t)\overline{z}(t). \tag{1.3}$$

Equation (1.3) can be written in the frequency domain as:

$$\overline{B}(f) = S(f) * \overline{Z}(f), \tag{1.4}$$

with $\overline{B}(f)$ and $\overline{Z}(f)$ being the Fourier transforms of $\overline{b}(t)$ and $\overline{z}(t)$, respectively. Passing $\overline{B}(f)$ through a nonlinear projection, it yields the ideal characteristics of the vibration signal $B_{nl}(f)$. Then, in the frequency domain, by minimizing the difference between $B_{nl}(f)$ and $\overline{B}(f)$:

$$min\,\|E(f)\| = min\,\left\|\overline{B}(f) - B_{nl}(f)\right\|, \tag{1.5}$$

iteratively through refining $\overline{Z}(f)$, $\overline{B}(f)$ will converge to the noise-free vibration signal. When it reaches the minimal value, $\overline{Z}(f)$ converges to $Z(f)$ and a good estimate of $B(f)$ is obtained as: $B(f) = S(f) * Z(f)$.

Lastly, the estimate is transformed back into the time domain to recover the noise-free vibration signal $b(t)$. The blind deconvolution de-noising scheme is illustrated in Figure 1.2 [24].

Note that the proposed scheme is implemented in the frequency domain and the nonlinear projection, which is derived from a nonlinear dynamic model, is also given in the same frequency domain [23, 24]. The blind deconvolution de-noising scheme was applied to vibration data derived from a faulted planetary gear plate. Results of 40% and 100% torque levels before and after de-noising indicate a significant improvement in the SNR. Improvement in the data SNR is accompanied by similar enhancements in the CI or features. The accuracy and precision of mappings relating CI propagation to fault dimension (crack length) growth is closely related to the performance of diagnostic and prognostic algorithms. To evaluate the quality of the CI, we define and employ two performance metrics. The first one is an accuracy
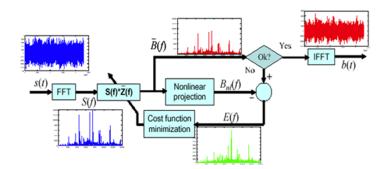
FIGURE 1.2: Blind deconvolution de-noising scheme.

measure and is defined as the correlation coefficient between the feature vector x and y as [23].:

$$CCR(x,y) = \sqrt{\frac{ss_{xy}^2}{ss_{xx}ss_{yy}}}, \tag{1.6}$$

where $ss_{xy} = \sum (x_i - \overline{x})(y_i - \overline{y})$, $ss_x x = \sum (x_i - \overline{x})^2$ and $ss_y y = \sum (y_i - \overline{y})^2$, respectively. The second is a precision measure called the Percent Mean Deviation (PMD) and defined by:

$$PMD(x,\tilde{x}) = \frac{\sum_{i=1}^{n} \frac{x_i - \tilde{x}_i}{\tilde{x}_i}}{n} \times 100, \tag{1.7}$$

where n is the number of entities in the feature vector x and $\tilde{x}$ its smoothed version.

1.2.2   Selection and extraction of condition indicators

Feature or condition indicator selection and extraction constitute the cornerstone for accurate and reliable fault diagnosis. The classical image recognition and signal processing paradigm of $data \rightarrow information \rightarrow knowledge$ becomes most relevant and takes central stage in the fault diagnosis case, particularly since such operations must be performed on-line in a real-time environment.

Fault diagnosis depends mainly on extracting a set of CI from sensor data that can distinguish between fault classes of interest, detect and isolate a particular fault at its early initiation stages. These features should be fairly insensitive to noise and within fault class variations. The latter could arise because of fault location, size, etc. in the frame of a sensor. *Good* features must have the following attributes:

- Computationally inexpensive to measure

- Mathematically definable

- Explainable in physical terms

- Characterized by large interclass mean distance and small interclass variance

- Insensitive to extraneous variables

- Uncorrelated with other features

Past research has focused on feature extraction; whereas feature selection has relied primarily on expertise, observations, past historical evidence, and understanding of fault signature characteristics. In selecting an "optimum" feature set, we are seeking to address such questions as: Where is the information? How do fault (failure) mechanisms relate to the fundamental "physics" of complex dynamic systems? Fault modes may induce changes in the energy, entropy, power spectrum, signal magnitude, among others.

Feature selection is application dependent. We are seeking those features, for a particular class of fault modes, from a large candidate set that possess properties of fault *distinguishability* and *detectability* while achieving a reliable fault classification in the minimum amount of time. Feature extraction, on the other hand, is an algorithmic process where features are extracted in a computationally efficient manner from sensor data, while preserving the maximum information content. Thus, the feature extraction process converts the fault data into an N-dimensional feature space, such that one class of faults is clustered together and can be distinguished from other classes. However, in general, not all faults of a class need N features to form a compact cluster. It is only the faults that are in the overlapping region between two or more classes that govern the number of features required to perform classification.

We have developed a hybrid methodology for feature selection and extraction that relies on physics-based modeling of the fault modes in combination with sensor data as the latter are streaming into our processor. The physics-based models, as previously described, employ a finite element analysis technique jointly with a nonlinear dynamic model of the failing component's behavior to guide the selection process. For example, in a typical helicopter main transmission gearbox, modeling of a crack (fault) on the planetary gear plate suggests that a "good" indicator may be computed from the meshing components in the frequency domain; i.e., by assessing the relative magnitudes of the dominant frequency components around a specific meshing frequency and those of the sidebands around them. Changes in the magnitudes are observed (dominants decreasing and sidebands increasing) as the crack grows. Figure 1.3 depicts the extraction process from accelerometer data [15, 22].

Thus, an insight into the physics of failure mechanisms, in combination with pre-processed data, provides a reasonable and systematic approach to feature selection and extraction. We will build on these concepts to address fault modes in aircraft systems; i.e., our selected testbed. Feature evaluation
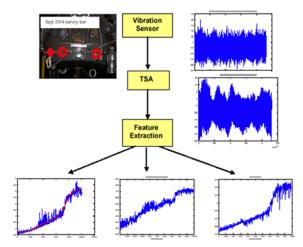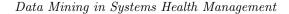
FIGURE 1.3: Feature extraction example.

and selection metrics include the similarity (or linear correlation) between the feature and the true fault (crack) size, based on the linear dependency between them. A feature is desirable if it shows a similar growth pattern to that of the ground truth data.

When multiple features are extracted for a particular fault mode, it might be desirable to combine or fuse uncorrelated features to enhance the fault *detectability* . We can take advantage of genetic programming algorithms to define an appropriate fitness function and using genetic operators to construct new feature populations from old ones.

1.2.3   The diagnostics and prognostics modules

The proposed scheme achieves robust component diagnosis by replicating multiple behaviors of a faulted system in a physics-based model. This procedure is illustrated in Figure 1.4. The simulated behaviors can be compared to particular instances of observed behaviors in an actual aircraft while in operation to determine the current fault or damage status of one of its subsystems, per the matching situation in the model. This is referred to as a "reverse engineering" approach.

We illustrate the modeling methodology through a specific example of a fault in the main transmission of a helicopter: a crack in the carrier plate of the planetary gearbox [8, 16]. We constructed simulations using a physics-based model that replicate the helicopter transmission's behavior under flight loads which then provide information on how vibration signals are expected to change when the crack is present. Actual tests are then used to observe
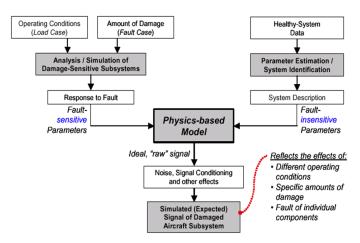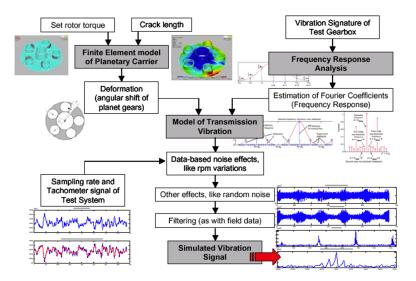
FIGURE 1.4: Suggested methodology for performing model-based simulation of faulted systems.

these changes and lead to the detection of the crack. The technique of Figure 1.4 is applied to this particular example as illustrated in Figure 1.5.

Simulations can provide information about which vibration characteristics show a relation with the crack length, and it becomes possible to estimate the size of a crack present in a component at a given instant. This is illustrated in Figure 1.6.

The prognosis task attempts to estimate how quickly the damage of an aircraft subsystem will progress. We take into consideration that progression of the damage depends on how the system will be used (damage progression rates may be affected by changes in environmental conditions, amount of load in the system, usage patterns), and that there is uncertainty in the estimated amount of damage when a fault is detected. We estimate the RUL or Time-to-failure (TTF) of the faulty component, as shown in Figure 1.7.

This novel modeling framework combines both physics-based principles and data-driven (measurement, models) techniques in a **hybrid setting** to provide a better understanding of the physics of failure mechanisms and, on that basis, support the derivation of optimal fault features and parameters needed for fault diagnosis and prognosis.

FIGURE 1.5: Application of a model-based technique for simulating the vibration of a faulted helicopter transmission.
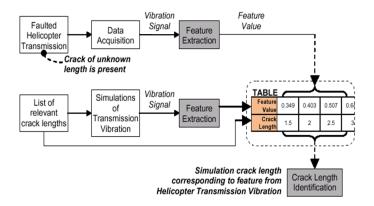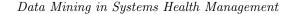

FIGURE 1.6: Application of the "reverse engineering" approach for performing model-based fault diagnosis in the helicopter transmission example.
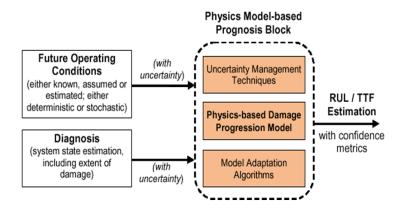
FIGURE 1.7: A general approach to realizing model-based prognostics.

1.3 Particle filtering algorithms in a combined model-based/data-driven framework for failure prognosis

The performance of a failure prognosis approach depends, to a great extent, on the ability of the dynamic model to mimic the behavior of the process under study. Linear and Gaussian dynamic models may help to describe this behavior satisfactorily when either the process complexity allows for it or when the time framework for long-term predictions is shortened. Most of the time, though, real processes require the inclusion of nonlinear dynamics or non-Gaussian stochastic components for an accurate description, especially when the time horizon required for the generation of dependable results is long enough to make evident any shortcomings introduced through linearization methodologies. For these reasons, a combined model-based/data-driven approach to prognosis not only should be capable of estimating the current condition of the system (and its model parameters), but also to adequately extrapolate the evolution of that condition in time.

1.3.1 Particle filtering algorithms and failure prognosis

Nonlinear Bayesian filters, and particularly sequential Monte Carlo methods (a.k.a. particle filters), provide a consistent theoretical framework to handle the problem of state estimation under the aforementioned conditions; i.e., to use noisy observation data to estimate at least the first two moments of a state vector governed by a dynamic nonlinear, non-Gaussian state-space model. Although we will not focus our discussion on the details associated to the implementation of particle filtering (PF) algorithms, it suffices to say

that these algorithms allow to approximate the *posterior* probability density $p(x_t/y_t)$ of the state vector x at time t, given a set of measurements $y_1, y_2, ..., y_t$ [1, 2, 4]. On the one hand, the *a priori* probability density is determined by the state dynamic model that describes the discrete-time system; as shown in (1.8), where U is a vector of external inputs to the system. Note that some of the components of the state vector x may represent unknown model parameters that have to be estimated in an online fashion.

$$\begin{cases} x_{t+1} = f(x_t, U_t, t) & \Leftrightarrow p(x_{t+1}/x_t, U_t) \\ y_t = h(x_t, t) & \Leftrightarrow p(y_t/x_t) \end{cases} \tag{1.8}$$

$$p(x_t/y_t) \propto p(x_t/x_{t-1}, U_{t-1}) \cdot p(y_t/x_t) \tag{1.9}$$

The *posterior* density $p(x_t/y_t)$, on the other hand, is then approximated using a set of $N >> 1$ weighted samples $\{w_t^{(i)}, x_t^{(i)}\}_{i:1\cdots N}$, $w_t^{(i)} \geq 0$ (also referred to as "particles") such that [2]:

$$p(x_t/y_t) \approx \sum_{i=1}^{N} w_t^{(i)} \cdot \delta(x_t - x_t^{(i)}). \tag{1.10}$$

As in the case of any adaptive prognosis scheme, it is assumed that there is at least one feature providing a measure of the severity of the fault condition under analysis (fault dimension). If many features are available, they can always be combined to generate a single indicator (with the help of techniques from the computational intelligence arena, for example). Thus, it is always possible to use state model (1.11), as a particular version of (1.8), to describe the evolution in time of the fault dimension:

$$\begin{cases} x_{1,t+1} = x_{1,t} + x_{2,t} \cdot F(x_t, t, U) + \omega_{1,t} \\ x_{2,t+1} = x_{2,t} + \omega_{2,t} \\ y_t = x_{1,t} + \nu_t, \end{cases} \tag{1.11}$$

where $x_{1,t}$ is a state representing the fault dimension under analysis, $x_{2,t}$ is a state associated with an unknown model parameter, U is a vector of external inputs to the system (load/stress profiles), $F(\cdot)$ is a general time-varying nonlinear function, ω_1, ω_2 and ν are white noises (not necessarily Gaussian). The nonlinear function F may represent a model based on first principles, a neural network, or even a fuzzy system [13].

State equation (1.11) provides the means to generate k-step ahead predictions of the expectation for the fault dimension, as well as to represent the evolution in time of the uncertainty that is associated to the state estimates. This uncertainty is characterized in the predicted conditional PDF $\hat{p}(x_{t+k}^{(i)}/x_t^{(i)})$, which describes the state distribution at the future time instant $t + k$ $(k > 1)$ when the particle $x_t^{(i)}$ is used as initial condition of the system.

Assuming that the current particle weights $\{w_t^{(i)}\}_{i:1...N}$ are a good representation of the state PDF at time t, then it is possible to approximate the predicted state PDF at time $t+k$, by using a weighted sum of kernel functions and the law of total probabilities, as it is shown in (1.12):

$$\hat{p}(x_{t+k}/x_{1:t}) \approx \sum_{i=1}^{N} w_t^{(i)} \cdot K_h(x_{t+k} - E[x_{t+k}/x_t^{(i)}]), \qquad (1.12)$$

where $K_h(\cdot)$ is a scaled kernel density function, which may correspond to the process noise pdf, a Gaussian kernel or a rescaled version of the Epanechnikov kernel [11, 14].

The resulting predicted state PDF contains critical information about the evolution of the fault dimension over time. One way to represent that information is through the computation of statistics (expectations, 95% confidence intervals), the Time-of-Failure (ToF) and the Remaining Useful Life (RUL) of the faulty system. A detailed procedure to obtain the RUL PDF from the predicted path of the state PDF is described and discussed in [14], although the general concept is as follows. The RUL PDF can be computed from the function of probability of failure at future time instants. This probability is calculated using both the long-term predictions and empirical knowledge about critical conditions for the system. This empirical knowledge is usually incorporated in the form of thresholds for main fault indicators, also referred to as the hazard zones.

In real applications, it is expected for the hazard zones to be statistically determined on the basis of historical failure data, defining a critical PDF with lower and upper bounds for the fault indicator (H_{lb} and H_{ub}, respectively). Since the hazard zone specifies the probability of failure for a fixed value of the fault indicator, and the weights $\{w_t^{(i)}\}_{i:1...N}$ represent the predicted probability for the set of predicted paths, then it is possible to compute the probability of failure at any future time instant (namely, the RUL PDF) by applying the law of total probabilities, as shown in (1.13). Once the RUL PDF is computed, combining the weights of predicted trajectories with the hazard zone specifications, it is well known how to obtain prognosis confidence intervals, as well as the RUL expectation [12, 14].

$$\hat{p}_{ToF}(t) = \sum_{i=1}^{N} w_t^{(i)} \cdot Pr(Failure/X = x_t^{(i)}, H_{ub}, H_{lb}) \qquad (1.13)$$

Equations (1.11), (1.12), and (1.13) can be used to show that the *a priori* state PDF for future time instants, and thus the time-of-failure (ToF) PDF, directly depends on the *a priori* probability distribution of the load profile for future time instants [13, 14]. Most of the times, long-term predictions assume that the latter distribution is a Dirac's delta function, which basically implies a deterministic function of time for future load profiles. Although this simplification helps to speed up the prognostic procedure, generating the

most likely ToF estimate, it does not consider future changes in operating conditions or unexpected events that could affect the remaining useful life of the system under analysis. Monte Carlo simulation can be used to generate ToF estimates for arbitrary a priori distributions of future load conditions, however it is not always possible to obtain these results in real-time. In this sense, PF-based prognostic routines not only provide a theoretical framework where these concepts can be incorporated, but also allow the use of uncertainty measures to characterize the sensitivity of the system, with respect to changes in future load distributions.

Furthermore, if a formal definition of mass probability is assigned to each possible stress condition, a ToF PDF estimate can be obtained as a weighted sum of kernels, where each kernel represents the PDF estimate of a known constant load. Indeed, if the *a priori* distribution of future operating conditions is given by:

$$\hat{P}(U = u) = \sum_{j=1}^{N} \pi_j \cdot \delta(u - u_j), \tag{1.14}$$

where $\{u_j\}_{i:1 \cdots N_u}$ is a set of deterministic functions of time, then the probability of failure at a future time t can be computed using (1.15).

$$\hat{p}_{ToF}(t) = \sum_{j=1}^{N_u} \pi_j \sum_{i=1}^{N} w_t^{(i)} \cdot Pr(Failure/X = x_t^{(i)}, H_{ub}, H_{lb}) \tag{1.15}$$

Equations (1.8)-(1.15) represent a suitable theoretical foundation for real time representation of uncertainty in a PF-based prognosis framework. They not only indicate how to use information from online feature measurements to update state estimates and parameters in empirical growth models, but also show how to use those those estimates to compute the predicted probability density distribution of the time of failure, assuming a statistical measure of uncertainty for system inputs and outputs [12, 13]. The next step is to determine how to use these empirical measures to anticipate the effect that input variations have on the faulty system, particularly in terms of the resulting RUL estimates.

1.3.2 Uncertainty measure-based feedback loops for the extension of remaining useful life

The main motivation behind the definition of uncertainty measures, for the outcomes of PF-based prognostic routines, is to characterize in real time the effects that changes in operating conditions may cause on the system RUL. This is, however, only the first step needed to solve a much more complex issue: to establish correction loops to extend the remaining useful life of a

process, based on the current condition of the system and a projection of its evolution in time.

The aforementioned concept is illustrated in Figure 1.8, which depicts a situation where the objective is to predict the evolution of a fault condition (detected at time t_{detect}) beyond the current time instant $t_{prognosis}$. In this case, the assumption of different stress profiles, for the future operation of the plant, may have a significant impact on the outcomes of prognostic algorithms for the system. The use of sensitivity measures, to characterize the effect of input uncertainty on the uncertainty associated to RUL estimates, provides a basis for the understanding of the modifications that the process requires to achieve the extension of its RUL. It is assumed, at this point, that the trivial solution to extend the RUL of a system (constant null load) is infeasible, since that would indicate that the system operation is terminated (e.g., an aircraft cannot stay aloft without a non-zero level of stress being exerted on the system). Moreover, a set of feasible stress profiles and operating points is assumed to be given.
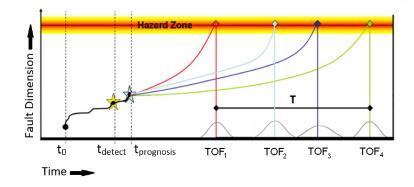

FIGURE 1.8: Predicted fault growth for different input stress levels.

The stress sensitivity is a measure of the change in uncertainty in the RUL prediction, as a function of the uncertainty in the stress profile (input to the system). Stress sensitivity is found by adding Gaussian i.i.d. white noise to the median stress level (U_{Base}, calculated among all feasible stress profiles) and then comparing the prognostic outcome with the RUL PDF that would be obtained when assuming the median stress level as a deterministic funtion of future time instants. This effect is illustrated in Figure 1.9 where the green kernels show U_{Base} and the resulting RUL_{Base} PDF, whereas the blue kernels show $U_{Base+\omega}$ and the resulting $RUL_{Base+\omega}$ PDF. Since U_{Base} is a deterministic function of time, then its *a priori* distribution is represented as a Diracs delta function. Stress sensitivity is measured in two ways, *dispersion sensitivity* (DS), defined in (1.16) and *confidence interval sensitivity* (CIS), defined in (1.17):

$$DS_\omega = \frac{stdev(RUL_{Base+\omega})}{stdev(RUL_{Base})}, \qquad (1.16)$$

$$CIS_\omega = \frac{Length(CI\{RUL_{Base+\omega}\})}{Length(CI\{RUL_{Base}\})}, \qquad (1.17)$$

where $RUL_{M+\omega}$ is the predicted RUL with a load factor of $U_{M+\omega}$ where $U_{M+\omega}(t) = U_M(t) + \omega(t)$ and $\omega(t)$ is Gaussian white noise. Measures based on the stress sensitivity concept provide a means of determining how adjustments on the system inputs will affect the RUL prediction, without the need of running individual simulations for all possible future stress profiles.

The main motivation behind the definition of uncertainty measures, based on the outcomes from PF-based prognostic routines, is to characterize in real-time the effects (in terms of the RUL of a system) that may be caused by changes in operating conditions. However, that is only the first step in a more complex problem: to establish correction loops aimed to extend the remaining useful life of a piece of equipment. In this sense, this section presents and analyzes a novel measure-based method that is proposed as a general approach to establish feedback correction loops aimed to lengthen the RUL of a nonlinear system. The method utilizes a PF-based prognosis framework to determine the baseline pdf estimate of the remaining useful life (RUL_{Base}) and then utilizes the sensitivity measures (DS and CIS) to determine an appropriate stress level that will extend the RUL of the component to the specified desired RUL (RUL_d). Two approaches to the method are outlined below: DS-based and CIS-based.
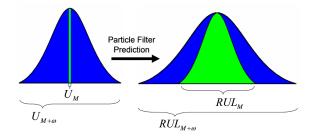

FIGURE 1.9: Illustration of PDF kernels, associated to the concept of stress sensitivity.

1.3.2.1   DS-based approach to RUL extension

Consider a baseline RUL PDF (RUL_{Base}) that is determined through PF-based prognostic routines using the expected future stress profile U_{Base}. The proposed DS-based approach to RUL extension uses knowledge of the dispersion sensitivity measure to extend the remaining useful life from $E[RUL_{Base}]$

to RUL_d by adjusting the stress factor to a safe level (U_d). To determine U_d, the standard deviation of the RUL PDF estimate which places RUL_d in the 95th percentile of the distribution, while maintaining a mean of $mean\{RUL_{Base}\}$, must be determined. This distribution is denoted as $RUL_{Base+\bar{\omega}}$, as shown in (1.18).

Using a linear fit, see Figure 1.10, to map the standard deviation of the stress to the standard deviation of the RUL PDF, it is possible to compute the standard deviation of the stress profile required to output a distribution of $RUL_{Base+\bar{\omega}}$ using (1.19). The standard deviation of this stress is then utilized to determine how much the baseline stress must be reduced in order to attain a remaining useful life of RUL_d, as seen in (1.20).

$$stdev\{RUL_{Base+\bar{\omega}}\} = \frac{RUL_D - E\{RUL_{Base}\}}{Z_{0.95}} \qquad (1.18)$$

$$stdev\{U_{Base+\bar{\omega}}\} = (\frac{stdev\{RUL_{Base+\bar{\omega}}\}}{stdev\{RUL_{Base}\}} - 1)\frac{stdev\{\omega\}}{DS - 1} \qquad (1.19)$$

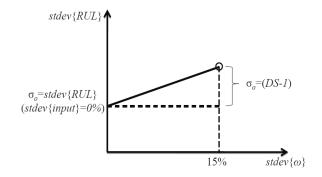$$U_d = U_{Base} - stdev\{U_{Base+\bar{\omega}}\} \qquad (1.20)$$

FIGURE 1.10: Linear mapping between standard deviation of stress profile and standard deviation of estimated RUL PDF.

1.3.2.2 CIS-based approach to RUL extension

Similar to the DS-based, the CIS-based approach to RUL extension uses knowledge of the confidence interval sensitivity to extend the RUL from $E[RUL_{Base}]$ to RUL_d by adjusting the stress factor to a safe level (U_d), given a PF-based estimate for RUL_{Base} that considers a baseline stress profile U_{Base}. To determine U_d, the confidence interval length of the RUL prediction which places RUL_d at the highest end of the confidence interval of the distribution, while maintaining a mean of $mean\{RUL_{Base}\}$, must be determined. This distribution is denoted as $RUL_{Base+\bar{\omega}}$, as shown in (1.21). Using a linear fit, see

Figure 1.11, to map the confidence interval length of the stress to the confidence interval length of the remaining useful life, the standard deviation of the stress required to output a distribution of $RUL_{Base+\bar{\omega}}$ is determined by (1.22). The standard deviation of this stress is then utilized to determine how much the baseline stress must be reduced in order to attain a remaining useful life of RUL_d, as seen in (1.23).

$$Length(CI\{RUL_{Base+\bar{\omega}}\}) = 2(RUL_D - E\{RUL_{Base}\}) \qquad (1.21)$$

$$stdev\{U_{Base+\bar{\omega}}\} = \left(\frac{length(CI\{RUL_{Base+\bar{\omega}}\})}{length(CI\{RUL_{Base}\})} - 1\right)\frac{stdev\{\omega\}}{CIS - 1} \qquad (1.22)$$

$$U_d = U_{Base} - stdev\{U_{Base+\bar{\omega}}\} \qquad (1.23)$$
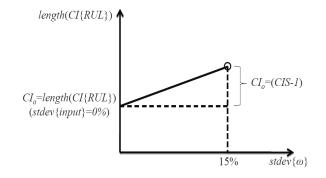

FIGURE 1.11: Linear mapping between the length of the confidence interval for stress profile and length of the confidence interval of estimated RUL PDF.

1.4 Case study: Load reduction and effects on fatigue crack growth in aircraft components

An appropriate case study has been designed to test and show the potential of the proposed feedback correction strategy. This case study uses data (from a seeded fault test) that describes a propagating fatigue crack on a critical component in a rotorcraft transmission system. This particular fault mode not only can lead to a critical failure condition in the aircraft, but also until

very recently there was no certain way to determine its existence save by a detailed off-line inspection; a procedure that involves a significant financial cost.

In this data set, the crack has been artificially grown until it reached a total length of 1.34 [inches], and after that the gearbox was forced to operate with input changes that included variations between 20% and 120% of nominal load in a 3 [min] ground-air-ground (GAG) cycle; see Figure 1.12. From material structure theory, it is well known that the crack growth evolution may be explained by using an empirical model such as the Paris' Law (1.24), given the proper set of coefficients [16]:
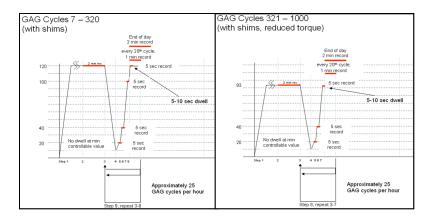

FIGURE 1.12: Loading profile (%) versus GAG cycles.

$$\frac{dL}{dt} = C(U_t \Delta K_t)^m \tag{1.24}$$

where L is the total crack length, C and m are material related coefficients, t is the cycle index, U_t is the parameter that includes the effect of crack closure during cycle t and K_t is the crack tip stress variation during the cycle t, measured in [MN/m$^{3/2}$]. The implementation of a prognostic framework based on model (1.24) necessarily requires the computation of two critical time-varying parameters: K_t and U_t. Now, the stress K_t may be estimated for a constant load (usually 100%) by using finite element analysis (FEA) tools such as ANSYS, for different crack lengths and crack orientations. In addition, if a proportional relationship is considered between the stress on the tips of the crack and the load applied to the system, then it is possible to relate both the current crack length and load variation (per cycle) with K_t. The problem is that this modeling effort, although helpful, is insufficient to estimate the evolution of the crack length. On one hand, the closure effect parameter U_t cannot be efficiently measured and only empirical approximations exist for certain materials. Even in the case of those materials, only upper and lower

bounds may be computed, and thus it is impossible to compute expectations and/or determine statistically the validity of confidence intervals.
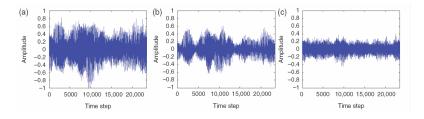

FIGURE 1.13: (a) the measured vibration signal s_t; (b) the recovered noise-free vibration signal b_t; (c) the noise signal n_t. Denoised vibration signal is used for purposes of feature computation.

The inclusion of process data, measured and pre-processed in real time, improves tremendously the prospect of what can be achieved in terms of prognostic results. The use of features based on the ratio between the fundamental harmonic and the sidebands in the vibration data spectrum [16] allows the implementation of the PF-based prognosis framework discussed in this chapter; see Figure 1.14. In that manner, not only it is possible to estimate the expected growth of the crack, but also the unknown closure parameter in crack growth model (1.24) and the RUL PDF, enabling the computation of statistics, expectations and confidence intervals. In fact, under this premise, (1.25) represents a suitable crack growth model to be used for real time state estimation purposes [14]:

$$\begin{cases} x_{1,t+1} = x_{1,t} + Cx_{2,t} \cdot ((\Delta K_t^{inboard})^m + (\Delta K_t^{outboard})^m) + \omega_{1,t} \\ x_{2,t+1} = x_{2,t} + \omega_{2,t} \\ y_t = h(x_{1,t}) + \nu_t, \end{cases} \tag{1.25}$$

where $x_{1,t}$ is the total crack length estimate at GAG cycle t, the state $x_{2,t}$ represents an unknown time-varying model parameter to be estimated (unitary initial condition), C and m are model constants related to material properties, and $\omega_{1,t}$, $\omega_{2,t}$ and ν_t are non-Gaussian white noises. ΔK_t (inboard/outboard) is the stress variation that is effective on the tips of the crack (a function of the load profile and the current crack length)and it can be computed through interpolation techniques. Information to be used in the interpolation procedure is obtained from off-line analysis of the system, using ANSYS, for a selected subset of operating conditions [16]. Process model (1.25) is fed with denoised feature data y_t [23], which is related with the fault dimension through a bijective nonlinear mapping $h(\cdot)$; see Figure 1.14. In this manner, this scheme allows to improve the state estimate every time a new denoised feature mea-

surement is included, helping to ensure the enhancement of both the precision and accuracy of RUL estimated through time.
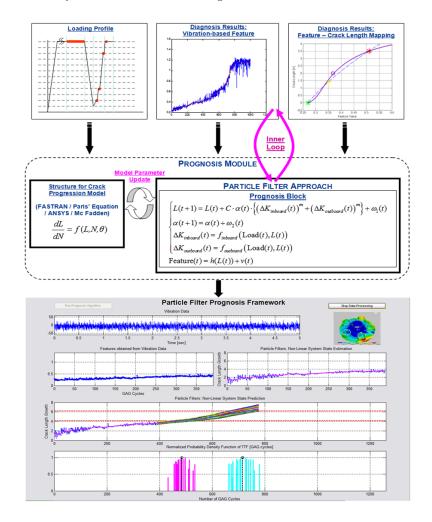

FIGURE 1.14: PF-based framework for prognosis: Crack growth in a planetary carrier plate. State estimation techniques are used to process denoised feature data, obtaining a ToF PDF estimate for selected thresholds in the feature value that define critical conditions for the system. The illustration shows the obtained results when two different thresholds are considered (magenta and cyan PDFs at the bottom)

Now, consider whithin this framework a situation where the pilot must remain airborne for a given amount of time in order to reach a safe landing destination. The RUL extension methods discussed in this chapter will provide

the pilot, or reconfigurable controller, with the information needed to adjust the load of the aircraft and reduce the stress on the failing component, with the purpose of extending the RUL to a desired time that ensures safe landing. Although a physics-based model for a system of these characteristics is a complex matter, it is possible to represent the growth of the crack (fault dimension) using the simplified model (1.25), where the nonlinear mapping functions are defined on the basis of an ANSYS stress model for the inner and outer tips of the fatigue crack [12, 14, 16].

Under this scenario, the use of algorithms capable of estimating the RUL by only analyzing vibration-based features becomes extremely attractive and would help to dramatically decrease operational and maintenance costs as well as avoid catastrophic events.

In the experiment, the baseline stress level was 120% of the maximum recommended torque. If this information is fed into the proposed PF-based prognosis framework, then the resulting ToF PDF (see cyan PDF in Figure 1.15), computed at the 300th cycle of operation, has an expectation of 594 cycles, a standard deviation of 12.44 cycles, and a confidence interval length of 38 cycles for $\alpha = 95\%$. If we were to compute the DS and CIS measures for this system at that particular cycle of operation (300th cycle), then it is necessary to compute the statistics of the ToF PDF that results after including uncertainty in the system input. Given that the implementation of a PF-based framework for failure prognosis allows to perform this task in a simple and efficient manner, it is possible, for example, to analyze the case when the input uncertainty is characterized by zero-mean Gaussian noise (standard deviation of 15% of maximum recommended torque). The resulting ToF PDF, has a standard deviation of 41.52 cycles and a confidence interval length of 142 cycles for $\alpha = 95\%$ (see magenta PDF in Figure 1.15).

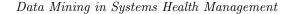Considered the aforementioned information, the dispersion sensitivity is found to be:

$$DS_{15\%} = \frac{stdev\{RUL_{Base+\omega}\}}{stdev\{RUL_{Base}\}} = \frac{41.52 cycles}{12.44 cycles} = 3.3362, \qquad (1.26)$$

and the confidence interval sensitivity is computed as

$$CIS_{15\%} = \frac{length(CI\{RUL_{Base+\omega}\})}{length(CI\{RUL_{Base}\})} = \frac{142 cycles}{38 cycles} = 3.7368. \qquad (1.27)$$

For this system the desired ToF is 714 cycles (RUL of 414 cycles). If we were to use the DS-based approach to RUL extension to suggest a correction in the stress profile for the system, then the standard deviation of the noise level required for cycle 714 to be located at the 95th percentile of the predicted magenta ToF PDF is found by:

$$\begin{aligned} stdev\{RUL_{Base+\bar{\omega}}\} \quad &= \frac{RUL_D - E\{RUL_{Base}\}}{Z_{0.95}} \\ &= \frac{714 - 594}{1.627} = 73.755. \end{aligned} \qquad (1.28)$$
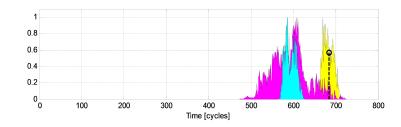
FIGURE 1.15: ToF PDF considering baseline (cyan), noisy(magenta), and desired (yellow) stress profiles for the problem of RUL estimation in the case study (cracked gear plate).

Inserting this value into (1.19) and solving for $stdev\{U_{Base+\bar{\omega}}\}$ yields a required standard deviation of 31.64% for the input stresses. Therefore in order to achieve the desired RUL of 714 cycles, the stress factor must be reduced by 31.64% from 120% to 88.36%.

Similarly, for the CIS-based approach to RUL extension, it is possible to estimate the required variation considering:

$$\begin{aligned} length(CI\{RUL_{Base+\bar{\omega}}\}) \quad &= 2(RUL_D - E\{RUL_{Base}\}) \\ &= 2(714 - 594) = 240. \end{aligned} \qquad (1.29)$$

Inserting this value into (1.22) and solving for $stdev\{U_{Base+\bar{\omega}}\}$ yields a required standard deviation of 29.13% for the input stress. Therefore in order to achieve the desired RUL of 714 cycles, the stress factor must be reduced by 29.13% from 120% to 90.70%. Compare 88.36% and 90.70% to the actual stress factor that results in a RUL of 714, which is 93%. Clearly, both approaches for stress correction suggest a modification, for the system input, that would have translated in an appropriate extension of the remaining useful life of the system.

1.5   Conclusions

This chapter presents theoretical and practical aspects associated to the implementation of a combined model-based/data-driven approach for failure prognostics based on particle filtering algorithms, in which the current estimate of the state PDF is used to determine the operating condition of the system and predict the progression of a fault indicator, given a dynamic state model and a set of process measurements. In this approach, the task of estimating the current value of the fault indicator, as well as other important changing parameters in the environment, involves two basic steps: the prediction step, based on the process model, and an update step, which incorporates the new measurement into the a priori state estimate.

This framework allows to estimate of the probability of failure at future time instants (RUL PDF) in real-time, providing information about time-to-failure (TTF) expectations, statistical confidence intervals, long-term predictions; using for this purpose empirical knowledge about critical conditions for the system (also referred to as the hazard zones). This information is of paramount significance for the improvement of the system reliability and cost-effective operation of critical assets, as it has been shown in a case study where feedback correction strategies (based on uncertainty measures) have been implemented to lengthen the RUL of a rotorcraft transmission system with propagating fatigue cracks on a critical component. Although the feedback loop is implemented using simple linear relationships, it is helpful to provide a quick insight into the manner that the system reacts to changes on its input signals, in terms of its predicted RUL. The method is able to manage non-Gaussian pdf's since it includes concepts such as nonlinear state estimation and confidence intervals in its formulation.

Real data from a fault seeded test showed that the proposed framework was able to anticipate modifications on the system input to lengthen its RUL. Results of this test indicate that the method was able to successfully suggest the correction that the system required. In this sense, future work will be focused on the development and testing of similar strategies using different input-output uncertainty metrics.

1.6   Glossary

ACMs: Automated contingency management systems

CI: Condition indicators

CIS: Confidence interval sensitivity

DS: Dispersion sensitivity

FDI: Fault detection and isolation

FEA: Finite element analysis

GAG: Ground-air-ground

PMD: Percent mean deviation

SMC: Sequential Monte Carlo

SNR: Signal-to-noise ratio

PDF: Probability density function

RUL: Remaining useful life

ToF: Time-of-failure

TTF: Time-to-failure

Bibliography

[1] A. Andrieu, C.and Doucet and Punskaya E. *Sequential Monte Carlo Methods for Optimal Filtering*. In *Sequential Monte Carlo Methods in Practice* , A. Doucet, N. De Frietas, and N. Gordon (Eds.) Springer-Verlag, NY, USA, 2001.

[2] M.S. Arulampalam, S. Maskell, N. Gordon, and T. Clapp. A Tutorial on Particle Filters for Online Nonlinear/Non-Gaussian Bayesian Tracking. *IEEE Transactions on Signal Processing*, 50(2), 2002.

[3] I. Dar and G. Vachtsevanos. Feature level sensor for pattern recognition using an active perception approach. In *Proceedings of IS&T/SPIE's Electronic Imaging '97: Science and Technology*, 1997.

[4] A. Doucet, N. de Freitas, and N. Gordon. *An introduction to Sequential Monte Carlo methods*. In *Sequential Monte Carlo Methods in Practice* , A. Doucet, N. De Frietas, and N. Gordon (Eds.) Springer-Verlag, NY, USA, 2001.

[5] A.D. Flint. A Prognostic Maintenance System Based on the Hough Transformation. *Transactions of the Institute of Measurement and Control*, 16(2):59–65, 1994.

[6] G. Hadden, P. Bergstrom, B. Bennett, G. Vachtsevanos, and J. Van Dyke. Shipboard machinery diagnostics and prognostics/condition based maintenance: A progress report. In *Proceedings of the Maintenance and Reliability Conference, MARCON 99*, pages 73.01–73.16, 1999.

[7] G. Hadden, G. Vachtsevanos, B. Bennett, and J. Van Dyke. Machinery diagnostics and prognostics and prognostics/condition based maintenance: A progress report, failure analysis: A foundation for diagnostics and prognostics development. In *Proceedings of the 53rd Meeting of the society for Machinery Failure Prevention Technology*, 1999.

[8] J. Keller and P. Grabill. Vibration monitoring of a uh-60a main transmission planetary carrier fault. In *Proceedings of the 59th Annual Forum AmericanHelicopter Society*, 2003.

[9] D. Kundur and D. Hatzinakos. Blind Image Deconvolution. *IEEE Signal Processing Magazine*, 13(3):43–46, 1996.

[10] K.A. Marko, J.V. James, T.M. Feldkamp, C.V. Puskorius, J.A. Feld-kamp, and D. Roller. pplication of neural networks to the construction of "virtual sensor and model-based diagnostics. In *Proceedings of ISATA 29th International Symposium on Automotive Technology and Automa-tion*, pages 133–138, 1996.

[11] C. Musso, N. Oudjane, and F. Le Gland. *Improving regularized particle filters*. In *Sequential Monte Carlo Methods in Practice* , A. Doucet, N. De Frietas, and N. Gordon (Eds.) Springer-Verlag, NY, USA, 2001.

[12] M. Orchard. *On-line Fault Diagnosis and Failure Prognosis Using Par-ticle Filters. Theoretical Framework and Case Studies*. VDM Verlag Dr. Mller Aktiengesellschaft and Co. KG, Saarbrcken, Germany, 2009.

[13] M. Orchard, F. Tobar, and G. Vachtsevanos. Outer Feedback Correc-tion Loops in Particle Filtering-based Prognostic Algorithms: Statistical Performance Comparison. *Studies in Informatics and Control*, 18(4):295–304, 2009.

[14] M. Orchard and G. Vachtsevanos. A Particle Filtering Approach for On-Line Fault Diagnosis and Failure Prognosis. *Transactions of the Institute of Measurement and Control*, 31(3-4):221–246, 2009.

[15] M. Orchard, B. Wu, and G. Vachtsevanos. A particle filter framework for failure prognosis. In *Proceedings of WTC2005 World Tribology Congress III*, 2005.

[16] R. Patrick, M. Orchard, B. Zhang, M. Koelemay, G. Kacprzynski, A. Ferri, and G. Vachtsevanos. An integrated approach to helicopter planetary gear fault diagnosis and failure prognosis. In *42nd Annual Sys-tems Readiness Technology Conference, AUTOTESTCON 2007*, 2007.

[17] T.D. Pebbles, M.A. Essawy, and S. Fein-Sabatto. An intelligent method-ology for remaining useful life estimation of mechanical components. In *Proceedings of the Maintenance and Reliability Conference, MARCON 99*, pages 27.01–27.09, 1999.

[18] R. Peled, S. Braun, and M. Zacksenhouse. A Blind Deconvolution Seper-ation of Multiple Sources with application to Bearing Diagnostics. *Me-chanical Systems and Signal Processing*, 14(3):427–442, 2000.

[19] M. Roemer, C. Byingston, G. Kacprzynski, and G. Vachtsevanos. An overview of selected prognostic technologies with reference to an inte-grated phm architecture. In *Proceedings of NASA Integrated Vehicle Health Management Workshop*, 2005.

[20] B.J. Rosenberg. The navy idss program: adaptive diagnostics and feed-back analysis-precursors to a fault prognostics capability. In *Proceedings of the IEEE National Aerospace and Electronics Conference, NAECON*, volume 3, pages 1334–1338, 1989.

[21] A. Saxena, B. Wu, and G. Vachtsevanos. Integrated diagnosis and prognosis architecture for fleet vehicles using dynamic case-based reasoning. In *Proceedings of AUTOTESTCON 2005 Conference*, 2005.

[22] B. Wu, A. Saxena, R. Patrick, and G. Vachtsevanos. Vibration monitoring for fault diagnosis of helicopter planetary gears. In *Proceedings of the 16th IFAC World Congress*, 2005.

[23] B. Zhang, T. Khawaja, R. Patrick, G. Vachtsevanos, M. Orchard, and A. Saxena. Application of Blind Deconvolution Denoising in Failure Prognosis. *IEEE Transactions on Instrumentation and Measurement*, 58(2):303–310, 2009.

[24] B. Zhang, T. Khawaja, R. Patrick, G. Vachtsevanos, M. Orchard, and A. Saxena. A Novel Blind Deconvolution De-Noising Scheme in Failure Prognosis. *Transactions of the Institute of Measurement and Control*, 32(1):3–30, 2010.